Competing Three-Dimensional Mechanisms in Compressor Flows

James V. Taylor & Robert J. Miller
Whittle Laboratory, University of Cambridge, United Kingdom
Email: jvt24@cam.ac.uk

Three-dimensional design is central to all modern compressor design systems, but many of these methods still rely on a two-dimensional and sectional view of aerodynamics at their core. This paper argues that this view fundamentally limits design by not considering the effect, on separation and loss, of the pressure gradient on the surface of the blade perpendicular to the meridional direction, here known as the transverse pressure gradient.

The first part of the paper details how altering the transverse pressure gradient, by changing a blade's 3D stacking, switches the way in which the blade aerodynamically "fails", from a open corner separation to a trailing edge separation. It also shows how the transverse pressure gradient significantly changes the blade profile loss.

In the second part, the effect of the transverse pressure gradient on the uncertainty inherent in the compressor design space is investigated. It is shown that as blade pitch-chord ratio is raised and the amount of 3D stacking is lowered the uncertainty of predicting a compressor's operating range is significantly raised. By increasing 3D stacking and the strength of the transverse pressure gradient it is shown that this uncertainty can be significantly reduced.

1 Introduction

Three-dimensional design is central to all modern compressor design systems, however, many of these methods still rely, at their core, on a two-dimensional and sectional view of aerodynamics. This paper will argue that this view fundamentally limits design because it does not capture the true loss mechanisms and fluid phenomena which shape the real design space.

At the early stage of the design process two-dimensional compressor aerodynamics plays a central role. Blade sections are often designed using quasi-3D methods such as MISES. These methods are typically used to both minimise profile loss and to inform pitch-chord ratio selection.

Later in the design process, during the 3D phase, designers often interpret the CFD in a 2D way. An example of this is the endwall diffusion parameter and the corner stall metric proposed by Lei et al. in [1]. At its heart this metric is two-dimensional, comparing the performance of a 2D section close to the endwall to the midspan. Even when 3D blade stacking is added to a design a 2D philosophy is employed. An example is the addition of compound lean, this is said to off-load the endwall sections relative to the midspan section.

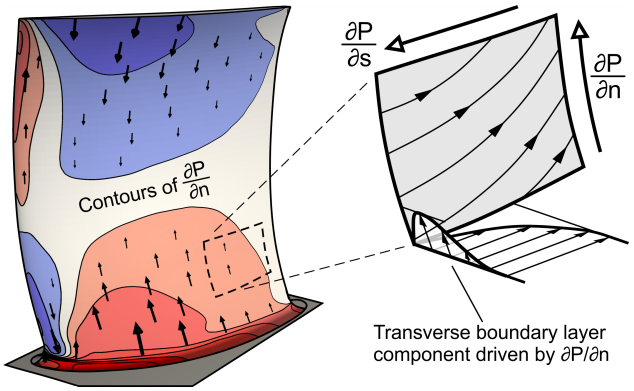

Fig. 1. TRANSVERSE SURFACE PRESSURE GRADIENT ON A COMPRESSOR BLADE

The difference between a 3D flow and a 2D flow is the capacity for a boundary layer to develop a transverse component. In a 2D flow the boundary layer is constrained to remain in the same plane as the freestream. The existence of the third dimension offers the boundary layer the possibility of "escape" laterally when it is confronted with a streamwise adverse pressure gradient (APG). This principle is illustrated in the right side of Figure 1, where regions of the boundary layer on the suction surface are able to flow in the spanwise direction.

This lateral "escape" mechanism means that the streamwise pressure gradient experienced by the boundary layer in a 3D flow is often lower than that experienced in a 2D flow. Considering aerodynamics in a two-dimensional and sectional way therefore misses the central behaviour that differentiates 2D and 3D flow.

The main outcome of 3D design should be to "manage" the transverse component of the boundary layer flow by controlling the transverse pressure gradient (TPG). The distribution of the transverse pressure gradient on a 3D blade design is shown in the left side of Figure 1. Increasing the

level of compound lean or sweep in a design will increase the strength of the transverse pressure gradient and promote stronger transverse boundary layer flow. Two-dimensional thinking completely ignores the central role of the transverse pressure gradient.

In this paper it is shown that there are two mechanisms that cause a rapid deterioration in performance. These will be termed "failure mechanisms" as they limit the useful incidence range of a blade. They are both 3D in nature and the onset of each mechanism can be controlled by manipulation of the transverse pressure gradient.

The first failure mechanism is an open corner separation. The occurrence of this mechanism will be later shown to be caused by infinite curvature of the limiting surface streamlines on the blade surface close to the endwall. It can be prevented by increasing the strength of the transverse pressure gradient as this acts to control the reversal of the limiting streamlines.

The second failure mechanism is a 3D trailing edge separation. This mechanism is traditionally thought to be 2D or quasi-3D. In this paper it will be shown to be caused by differential transverse migration of boundary layer fluid relative to the freestream. Once again the transverse pressure gradient is directly responsible for controlling the magnitude of this differential migration.

It will also be shown in this paper is that the loss mechanisms which control the design incidence performance of the blade are 3D. This means that the presence of the transverse pressure gradient makes the profile loss 3D in nature and therefore it cannot be predicted using 2D or quasi-3D methods, even at the design flow condition.

The one remaining problem with this novel approach to 3D design is uncertainty. CFD results may drive the designer to take out some compound lean or to remove blades in the search for improved performance. However, the designer is always uncertain of whether the numerically predicted benefits will be achieved in reality. This question is answered in the second part of the paper.

The design space described by simultaneous variation of 3D stacking and of pitch-chord ratio is explored experimentally. It is shown that the design space is split into two regions based on the underlying 3D failure mechanisms described above. In the first region the uncertainty is high and the designer must seek extensive experimental validation of the design. In the second region the uncertainty is shown to be low and the designer should have more confidence in being guided by the predictions of the CFD.

2 Method

The datum stator geometry was designed to operate at a Mach number of 0.3 and a Reynolds number of 350,000. The aspect ratio is 1.1 and the hub to tip ratio is 0.85. The blade has 20° of true lean and 4° of true sweep at the hub as defined in [2].

A matrix of 15 blades which varied both pitch to chord ratio and 3D stacking was tested. Three levels of pitch-chord ratio were selected; 100%, 108% and 116% of the datum value. The 3D stacking profiles are scaled linearly from the datum design in five levels; 30%, 70%, 100%, 130% and 170%. This scaling results in blades leant perpendicular to the chord line with angles at the hub of 6°, 14°, 20°, 26° and 34°. Sweep parallel to the chord line gives angles at the hub of 1.2°, 2.8°, 4°, 5.2° and 6.8°.

Numerical

The CFD results presented in this paper are all computed using TURBOSTREAM. It is a structured multi-block RANS solver based upon TBLOCK and implemented for parallel GPU operation. Further details and validation are given in [3]. Most solutions are steady simulations of the rotor and stator rows coupled with a mixing plane. Solutions which differ from this standard configuration are detailed in the text. An experimental area traverse of the IGV exit is used as the boundary condition at the rotor inlet. The turbulence model used was the Spalart-Allmaras method [4]. The meshing process is automated using AUTOGRID. The total cell count for the two rows is 3.1 million with 105 spanwise points in both blades and 19 in the rotor tip gap. y^+ is lower than 1 on all walls at all operating points. In the stator row a butterfly fillet topology was used at both hub and casing to ensure no discontinuity in angle and to improve the accuracy of the flow in the endwall suction surface corner. Transition was not modelled and the code considers the flow fully turbulent on all surfaces.

Experimental

Experimental testing was undertaken on the Gibbons compressor at the Whittle Laboratory. The facility has been upgraded to allow a rapid rate of testing. 3D printed UV cured resin cassettes are used to make up a sector or entire row of stator blades. It is possible to change a sector of stator blades in under ten minutes.

The stator and rotor hub platforms are sealed to ensure that no leakage path exists between the rows. Experimental results given in this paper are based upon stator inlet and exit traverses undertaken with a five-hole pneumatic probe. The ratio of probe diameter to span is 1.8% and the stator exit traverse is taken 0.25 chords downstream of the trailing edge. Stator geometry is replaced in sectors of 1/5 of an annulus, equivalent to 15 blades, the central two blades are traversed. Static-static stator characteristics are measured using 36 pneumatically averaged casing tappings spaced over the central three pitches of the 1/5 annulus sector at both inlet and exit of the stator row.

3 3D Blade Design

The purpose of the 3D design method used in this study is to vary the transverse pressure gradient on the blade while holding the spanwise loading distribution constant. This differs from the traditional methods of 3D design which use compound lean and sweep to vary both the transverse pressure gradient and spanwise loading distribution. The new design method is specifically aimed at decoupling these two

effects. It allows the designer to hold the spanwise loading distribution constant and study the transverse pressure gradient in isolation.

An iterative design process is required to vary the transverse pressure gradient independently of the spanwise loading distribution. The sweep and lean profile is imposed and then 3D CFD is used iteratively to achieve the desired loading distribution at each spanwise location. The system has free control over the camber distribution and metal angles. The system also maintains, at all spanwise locations, between all designs: local incidence, through the position of the stagnation point, chordwise position of peak suction and the shape factor distribution and magnitude at the trailing edge. The spanwise distribution of blade turning is shown to be constant for three different designs in Figure 2.

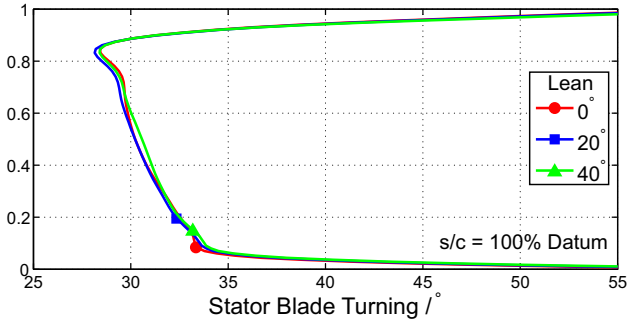

Fig. 2. SPANWISE DISTRIBUTION OF FLOW TURNING (CFD)

Contours of the transverse pressure gradient on the suction surface are shown in Figure 3. It is shown that the primary effect of lean and sweep is to cause a large increase in the strength of the transverse pressure gradient between the leading edge and 50% chord.

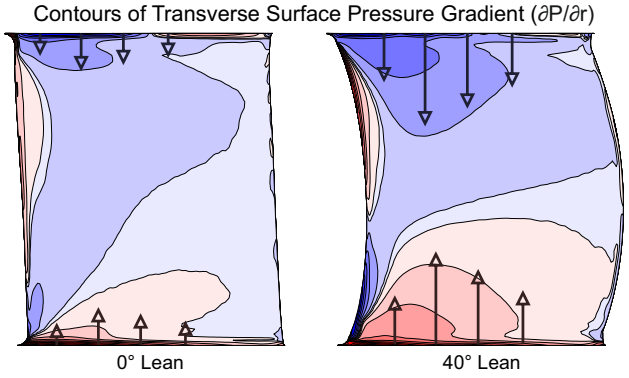

Fig. 3. EFFECT OF COMPOUND LEAN ON THE STRENGTH OF THE TRANSVERSE SURFACE PRESSURE GRADIENT (CFD)

This new method of 3D design conflicts with the traditional model used to interpret the effect of compound lean. Figure 4 shows both the traditional model and the new model. The figure shows a constant chord slice through the blade row. Cross-passage isobars are known to cluster tighter to the suction surface. The traditional model for compound lean aims to exploit this effect; moving the ends of the suction surface closer to the pressure surfaces puts them into regions of lower cross passage pressure gradient. This reduces the number of isobars betweens suction and pressure surface in the endwall while raising the number at midspan. The traditional model states that compound lean acts to "off-load" the endwalls and "load-up" the midspan.

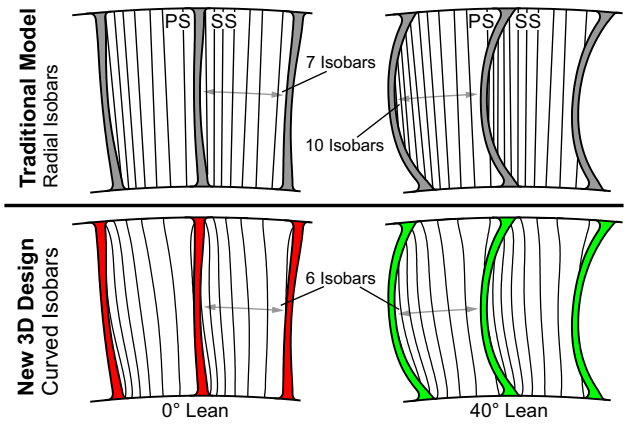

Fig. 4. CONTRAST BETWEEN TRADITIONAL MODEL USED TO INTERPRET LEAN AND THE NEW 3D DESIGN METHOD (CFD)

The effect of the new method of 3D design, employed in this paper, on the isobars, is shown in the lower half of Figure 4. In this case the isobars have been extracted from CFD. It can be seen that the isobars are not radial in reality, they curve as they approach the endwalls. The iterative design method controls curvature of the isobars to ensure that at all spanwise locations the number of isobars is independent of the level of compound lean. The results of Figure 3 and Figure 4 demonstrate that the new design method allows the transverse pressure gradient to be varied independently of the spanwise loading distribution.

The decoupling of the two effects of 3D design is central to this paper. It allows the impact of the transverse pressure gradient to be studied independently of the streamwise surface pressure gradient. Ideally all designers should have independent control of both the transverse and streamwise surface pressure gradients in this way.

4 3D Flow Mechanisms

Altering the strength of the transverse pressure gradient on a blade has a significant effect on both its incidence range and design incidence loss. The top half of Figure 5 shows the "loss loops" for three blades with different transverse pressure gradients as computed with 3D CFD. The bottom half shows contours of loss coefficient downstream of the blades with the highest and lowest transverse pressure gradients.

Three main effects of the changes to transverse pressure gradient can be observed. The first effect occurs at moder-

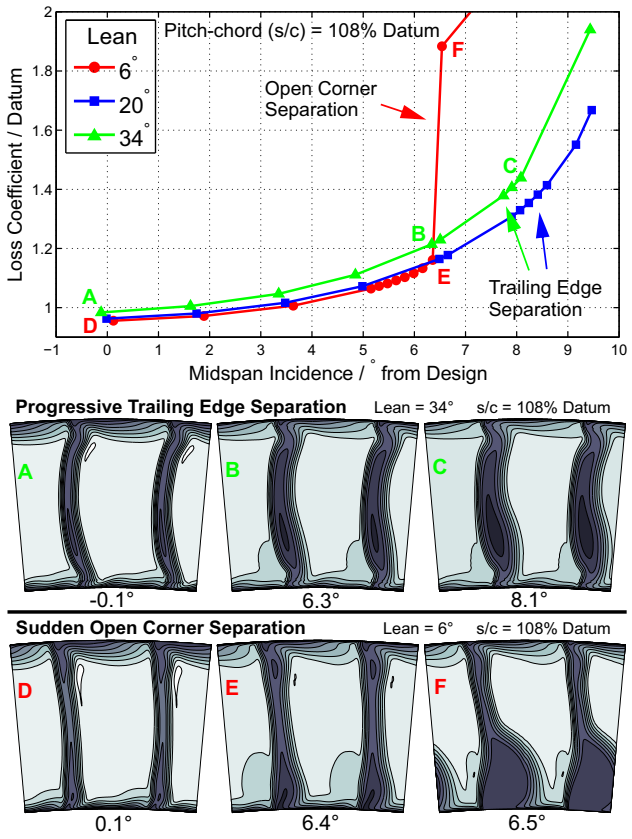

Fig. 5. TOP: BLADE LOSS VARIATION WITH INCIDENCE. BOTTOM: CONTOURS OF STATOR EXIT LOSS COEFFICIENT (CFD)

ate to high levels of transverse pressure gradient (20° and 34° lean). At these levels of transverse pressure gradient the blade fails progressively as incidence is raised. The failure mechanism responsible is that of a trailing edge separation on the suction surface away from the endwall, this can be seen in the contours plotted in the bottom half of Figure 5. As lean is increased from 20° to 34° the increase in the strength of the transverse pressure gradient acts to reduce the blade's incidence range.

The second effect occurs at low levels of transverse pressure gradient (6° lean). At these levels of transverse pressure gradient the blade fails suddenly at a critical incidence. The failure mechanism responsible is that of a sudden opening of the hub corner separation. This can also be seen in the contours of Figure 5. As lean is reduced from 20° to 6° the reduction in the strength of the transverse pressure gradient causes the switch from progressive failure to sudden failure.

The final effect occurs at design incidence. As the transverse pressure gradient is raised the total loss increases. This is surprising and counter to the prevailing wisdom that compound lean, especially in low levels, acts to reduce blade loss. The mechanism responsible for this is an increase in the profile loss.

In the remainder of this section the 3D mechanisms which cause each of these effects is discussed in more detail.

3D Trailing Edge Separations

At moderate to high levels of transverse pressure gradient the blade fails progressively with incidence. The failure is caused by a 3D trailing edge separation. The incidence at which the separation is initiated is observed to reduce as the strength of the transverse pressure gradient is raised. This behaviour is unexpected as the spanwise loading distribution remains constant in all cases.

The underlying structure of the 3D trailing edge failure is shown in Figure 6. At the design incidence the suction surface is attached. As incidence is raised a trailing edge separation initiates away from the endwall, it increases in spanwise and chordwise extent as incidence is raised further.

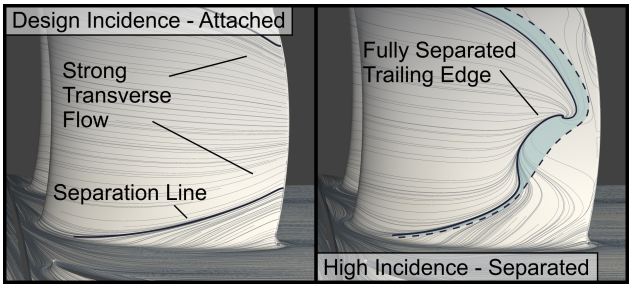

Fig. 6. STRUCTURE OF 3D TRAILING EDGE SEPARATION (CFD)

The cause of the progressive worsening of the trailing edge separation with increased strength of transverse pressure gradient can be seen in the right hand side of Figure 7. The figure shows the shape factor of the trailing edge boundary layer extracted from the 3D CFD. As lean is increased the shape factor at the trailing edge of the suction surface boundary layer rises, moving the design closer towards separation. The initial separation is observed to occur at around 20% to 30% span where a local peak in shape factor occurs.

To determine how accurate the 3D CFD was at predicting the change in the trailing edge shape factor with increased transverse pressure gradient the boundary layer of three blades were traversed using a micro flattened total pressure probe. A comparison of experiment and CFD is shown in Figure 7. The CFD was found to under predict the absolute value of shape factor by 0.15 but the CFD does predict the correct trend and magnitude of shape factor change with increasing transverse pressure gradient.

The cause of the rise in boundary layer trailing edge shape factor with increased transverse pressure gradient can be seen in Figure 8. Two blades are shown, one with a low transverse pressure gradient (6° lean) and one high (34° lean). The surface limiting streamlines on the suction side are shown in both cases. As the transverse pressure gradient is raised the stream tube contraction of the boundary layer fluid increases. This metric is called the surface contraction ratio (SCR). It should be noted that the SCR differs from AVDR because it affects the boundary layer alone.

The impact of the transverse pressure gradient on the boundary layer profile, at a point on the suction surface is

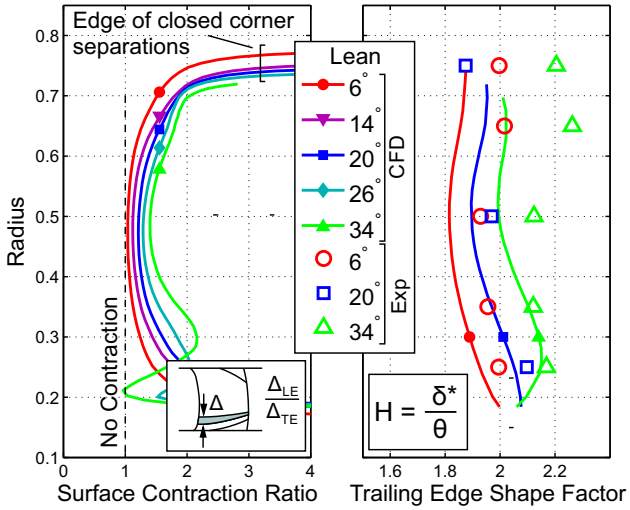

Fig. 7. EFFECT OF TRANSVERSE SURFACE PRESSURE GRADIENT. LEFT: ON SURFACE CONTRACTION RATIO. RIGHT: ON TRAILING EDGE SHAPE FACTOR (CFD+EXP)

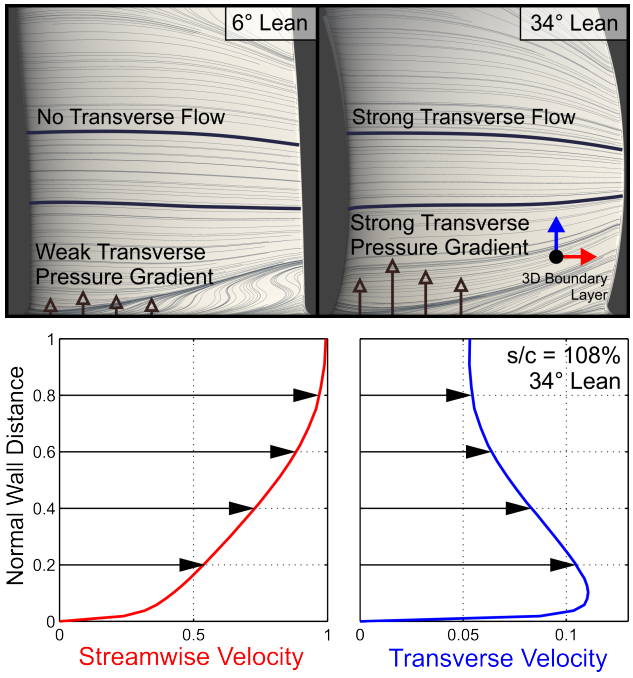

Fig. 8. EFFECT OF TRANSVERSE SURFACE PRESSURE GRADIENT ON TRANSVERSE BOUNDARY LAYER FLOW (CFD)

shown in the lower half of Figure 8. The inner part of the boundary layer has a lower streamwise momentum, thus under the effect of the transverse pressure gradient it is overturned towards midspan more than the outer part of the boundary layer. This can be seen in the component of transverse velocity. It is only through this differential overturning of the boundary layer in the transverse direction that the boundary layer shape factor is raised as in Figure 7. The spanwise distribution of SCR is plotted on the left hand side of Figure 7 for the designs of different transverse pressure gradient. The SCR is a direct measure of the rate of the low streamwise momentum overturning close to the surface, thus is it the most accurate metric for estimating the degradation of the boundary layer due to the effect of transverse boundary layer flow.

The size of this effect is significant. Raising compound lean from 6° to 34° raises the maximum shape factor of the boundary layer at the trailing edge by 0.3. Many industrial design processes use quasi-3D coupled boundary layer methods, such as MISES, to tailor their pressure distributions and thus to tailor the trailing edge shape factor of the boundary layer. By ignoring the surface contraction ratio these design processes significantly over estimate the health of the trailing edge boundary layer.

Open Corner Separations

At lower levels of transverse pressure gradient the blade fails suddenly with increased incidence. The failure is caused by a sudden opening of a corner separation. The critical incidence at which the corner separation opens is observed to drop as the strength of the transverse pressure gradient is reduced. The remainder of this section explains the mechanism responsible for the opening of the corner separation and presents a metric by which designers can judge how close a blade is to the onset of failure.

The underlying structure of the corner separation is shown in Figure 9. At design incidence the suction surface is attached and the corner separation is closed, however a small region of flow reversal on the surface is observed to occur in the corner close to the hub endwall. As the incidence is raised an abrupt switch in flow topology occurs, marked by the formation of a large separation surface. This is the opening of the corner separation.

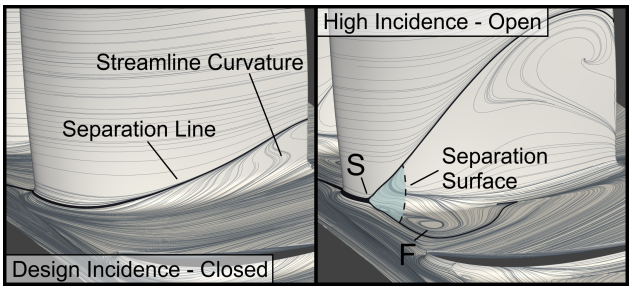

Fig. 9. STRUCTURE OF CORNER SEPARATIONS (CFD)

The presence of the separation surface is the single feature which distinguishes between a closed corner separation and the open type. The “separation surface” divides the flow in the passage as shown in the right panel of Figure 9. At the root of the separation surface are two critical points. On the fillet there is a saddle point marked as “S” and on the endwall there is a focus marked “F”. Closed corner separations are identified only by the presence of their “separation line”, this can exist without any reversed flow. A complete definition of 3D separations lines and surfaces is given by Délery in [5]. For the flow topology to switch from a closed to an

open separation requires the production of this saddle point and focus pair.

The effect of the transverse pressure gradient on the structure of the closed corner separations can be seen in Figure 10. It shows a blade with low and high transverse pressure gradient (6° and 34° lean). In the 6° lean case a region of severe streamline curvature is observed close to the hub. It will be shown that this is the region from which the separation surface originated. In the 34° lean case the region of streamline curvature is no longer present. This improvement in the "health" of the closed corner separation in the hub corner is a direct result of the stronger transverse pressure gradient promoting the migration of low streamwise momentum boundary layer fluid up the suction surface towards midspan.

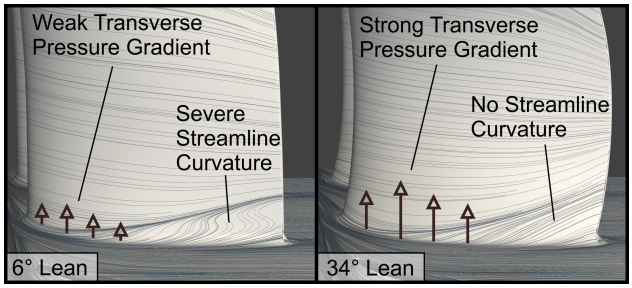

Fig. 10. EFFECT OF TRANSVERSE SURFACE PRESSURE GRADIENT ON THE CLOSED CORNER SEPARATION (CFD)

In order to investigate the significance of the severe streamline curvature as an origin for the separation surface an unsteady CFD prediction of a sector of stators was undertaken. The calculation modelled the transient process where the closed corner separation opens. The domain was made up of 6 stators of the datum pitch to chord ratio and a lean of 6°. The upstream IGV and rotor rows were also included with sliding planes. A single stator in the 6 was modified to have 1% less lean than the others. This ensures realism in that only one stator reaches its critical incidence before the rest.

Figure 11 shows the topology of the corner separation just before and after the critical incidence at which the separation surface and the associated saddle point and focus pair were formed. In the top panel the curvature of the reversing surface streamlines is severe. This is caused by both the streamwise adverse pressure gradient and cross passage migration of low momentum endwall boundary layer fluid into the suction surface corner at this high incidence condition. The region of most extreme surface curvature occurs at approximately 40% chord on the fillet.

The bottom panel of Figure 11 shows the surface limiting streamlines at an incidence slightly above the critical value. The curvature is observed to become infinitely sharp. This promotes the formation of the saddle point and focus pair and therefore the separation surface.

In order to interpret the significance of this region of the flow in forming the open corner separation from the closed

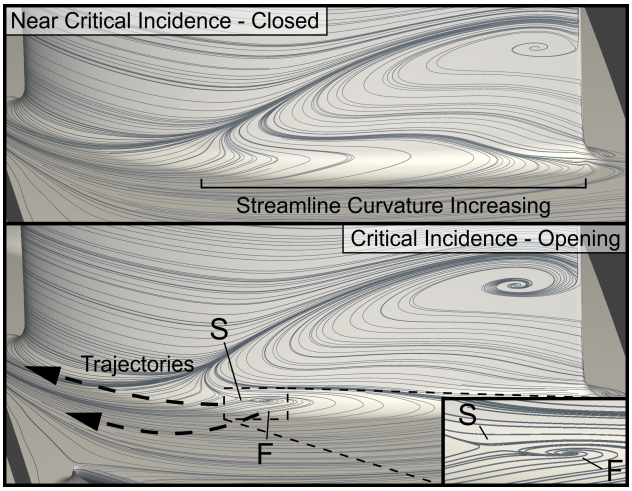

Fig. 11. INSTANTANEOUS SNAPSHOTS OF THE LIMITING SURFACE STREAMLINES BELOW AND ABOVE THE CRITICAL INCIDENCE (CFD)

type it is necessary to refer to the theory of critical points first published by Poincaré in [6] and recently applied to corner separations in compressor blades by Gbadebo et al in [7]. Two parts of this theory are significant to explain the phenomena: Firstly, critical points, such as foci, saddles and nodes, can only form from other regions of singular shear stress. Secondly, the number of critical points in the flow field must obey Equation 1 at all instants in time. The symmetry of this equation results in the production of the saddle point and focus pair together.

$$\sum(Foci + Nodes) - \sum Saddles = 0 \qquad (1)$$

The saddle point and focus pair originate from the region of infinitely sharp streamline curvature located on the fillet. The production of the two critical points is shown clearly in the lower panel of Figure 11, an instantaneous snapshot of the limiting surface streamlines. This pair of points has a separation line running between them. This new line marks the contact of the separation surface with the endwall. Through this mechanism the separation surface is able to form from the centre of the blade suction surface. This means that the failure mode occurs suddenly without warning.

Once the two critical points have formed, the flow becomes unstable and unsteady and moves swiftly to achieve a new stable operating point. Ultimately the saddle point moves forward toward the leading edge while the focus separates from it to sit on the hub endwall. This is the case shown in the right hand side of Figure 9, where the separation surface blocks a significant portion of the passage. This results in the collapse of the blade loading. Once an open separation has formed in one passage the local blockage increases incidence on the neighbouring passage. The next open separation is then able to form as the neighbouring passage's critical incidence has been exceeded.

The connection between the regions of severe surface streamline curvature and the formation of open corner separations offers the possibility of a metric for determining how close a given design is to forming an open separation. To be of use to designers it must be possible to extract such a metric from either CFD or experiment.

The metric chosen is called the "corner shape factor". As a concept it is analogous to a 2D boundary layer shape factor in that it is purely defined by the flow "shape". A metric could be based on the peak surface streamline curvature but this is difficult to measure with any certainty. An alternative method was therefore developed which could be extracted robustly from both CFD and experiment. The method is shown in Figure 12. The corner shape factor is defined as the angle between the forwards facing flow vector ($V1$) and the reversed flow vector ($V2$). The corner shape factor varies between 0 and π. As the angle tends towards π the local streamline surface curvature tends towards infinity and the saddle and focus point pair form.

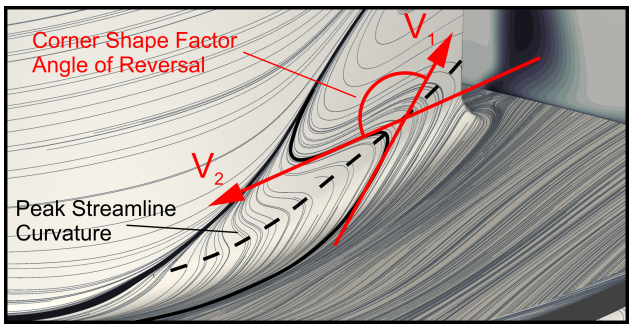

Fig. 12. DEFINITION OF THE CORNER SHAPE FACTOR (CFD)

The corner shape factor characterises the closed corner separation, and measures directly the proximity to instability, another parameter that in the past has been used to characterise this type of flow is the endwall loss. Figure 13 shows the new metric plotted against endwall loss coefficient calculated in the 20% mass flow closest to the hub. The use of the corner shape factor in characterising corner separations can be clearly seen. The plot includes all 15 geometries at all incidences. The corner shape factor ceases to have meaning once an open corner separation has formed and these results are not plotted. It should be noted that once the open separation has formed the endwall loss exceeds that of the datum by 3 times.

Figure 13 also shows the effect of the transverse pressure gradient. All the blades with 34° of lean have a hub corner shape factor of less than $\pi/8$ at all incidences; while all the designs with 20° lean have a hub corner separation of only less than $3\pi/8$ at all incidences. The power of the corner shape factor is in its ability to determine a design's proximity to forming an open corner separation. The authors propose this metric to be used during design of 3D blades in a similar way to how boundary layer shape factor is used in the design of blade sections. i.e. as a measure of the design's proximity to separation.

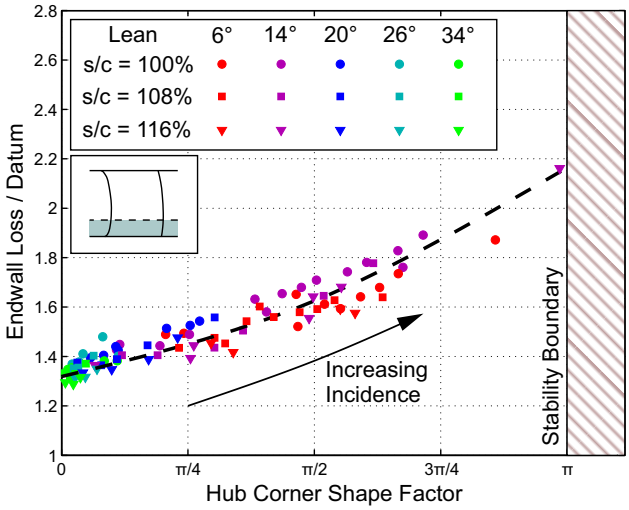

Fig. 13. VARIATION OF ENDWALL LOSS WITH CORNER SHAPE FACTOR AT ALL OPERATING POINTS (CFD)

Design Loss

Increasing the strength of the transverse pressure gradient raises the total loss at design incidence. The top panel of Figure 14 shows the experimentally measured stator exit loss coefficient for the designs with 6° and 34° of compound lean. The change in loss coefficient between the two cases, for both experiment and CFD is shown below the figure. The first point to note is that between 20% and 80% span the loss in the stator wake is much greater for the 34° lean case than for 6° lean case. This is however offset to some degree by the 6° lean blade having a high loss in the corners and on the endwall.

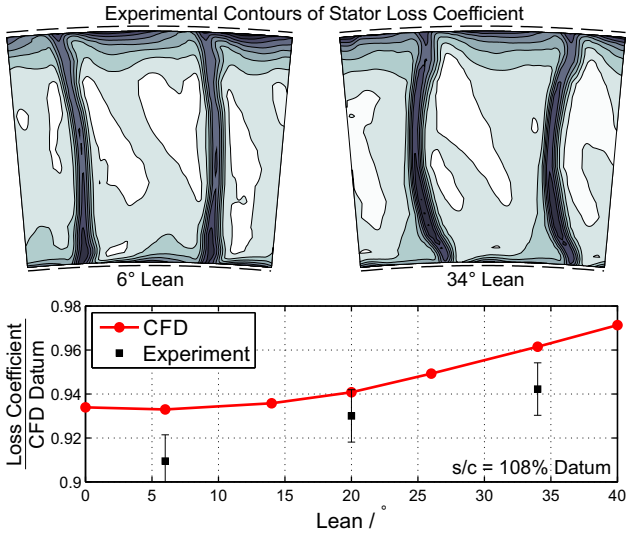

Fig. 14. TOP: VARIATION OF LOSS STRUCTURES. BOTTOM: VARIATION OF TOTAL LOSS WITH LEAN (CFD+EXP)

The rise in total blade loss coefficient is shown in the bottom panel of Figure 14. The increase in compound lean (6° to 34°) is predicted by the CFD to increase the total loss by 2.7%. The experimental results predict a rise of 3.4%. It is clear from both the experimental and numerical results that any increase in the strength of the transverse pressure gradient will increase the total loss. The remainder of this section will investigate the root cause of this loss increase.

The effect of increasing the transverse pressure gradient can be seen to increase the loss between 20% and 80% span in Figure 14. There are two possible causes of this rise. The first is that as compound lean is raised there is an increase in the spanwise migration of loss towards midspan; the increase in loss is due to redistribution. The second is that the transverse pressure gradient introduces a new loss mechanism.

To decouple these two mechanisms a stream tube tracking method, shown in Figure 15, is used. The 3D profile loss is defined as the loss which is generated in the central 60% of mass flow in the passage. The central 60% mass flow is bounded by two stream surfaces at the 20% and 80% spanwise mass flow locations. The surfaces are axisymmetric upstream of the stator. By tracking these stream surfaces through the row the effect of loss generation can be studied independently of the mechanism of loss redistribution.

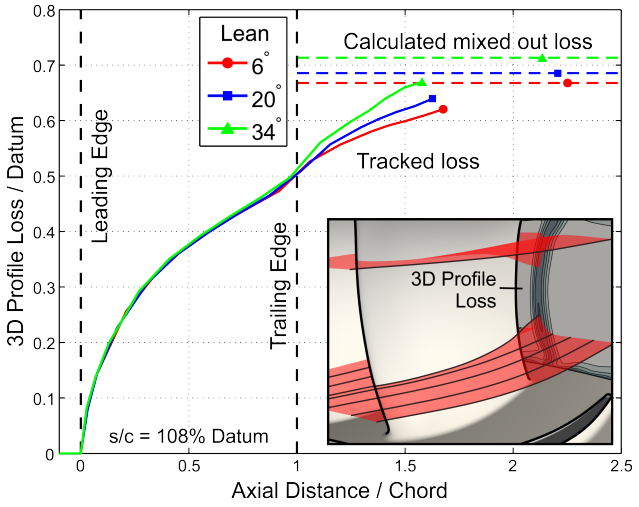

Fig. 15. AXIAL DEVELOPMENT OF 3D PROFILE LOSS THROUGH THE STATOR ROW (CFD)

Figure 15 shows that increasing lean has no effect on the 3D profile loss generated within the stator passage. The significant increase in loss is observed to occur downstream of the trailing edge in the region of wake mixing. Figure 15 also shows the mixed out loss calculated just downstream of the trailing edge. The mixed out loss is calculated by mixing the 3D profile loss region at the trailing edge circumferentially and mass averaging radially. This increased mixing loss would be responsible for an increase in total loss coefficient of 5.1%. However, an increased lean causes a reduction in endwall loss equivalent to a reduction in 2.4% of total loss. Thus between the 6° and 34° lean designs the total loss increases by 2.7% as per the CFD results in Figure 14.

The increase in wake mixing loss is caused by a change in the "shape" of the stator wake at the trailing edge. Two possible causes of "shape" change exist. The wake's two-dimensional (circumferential) shape could have changed or the wakes length (spanwise) length could have changed.

The impact of the change in "shape" of the 2D circumferential wake profile can be calculated directly from the trailing edge shape factor H_{32}. H_{32} is the ratio of the energy to momentum thickness of the boundary layer. Its value at the trailing edge sets the ratio of the blade's attached loss to total mixed out loss. Rotta in [8] and Wieghardt in [9] determined a unique relationship between H_{12} and H_{32}. Both results are presented by Schlicting in [10]. Figure 16 shows the results reported by Rotta and Wieghardt and the three CFD and experimental cases. It is shown that as the strength of the transverse pressure gradient is increased, transverse flow on the suctions surface causes H_{12} to rise and H_{32} to fall.

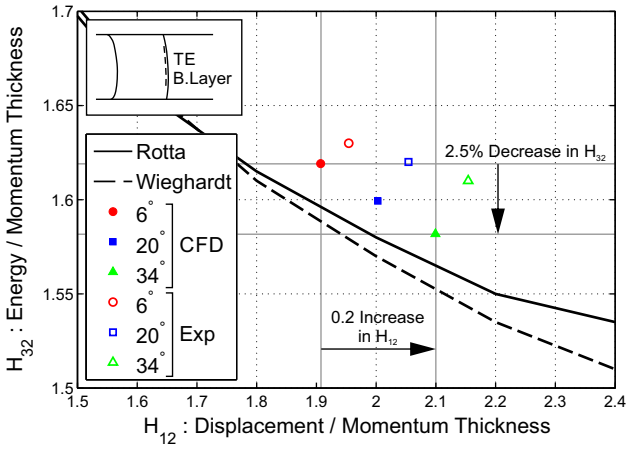

Fig. 16. THE RELATIONSHIP BETWEEN BOUNDARY LAYER SHAPE FACTORS (CFD+EXP)

Changing lean from 6° to 34° was shown in the previous section to increase H_{12} at midspan by 0.2. Figure 16 shows that this corresponds to a 2.5% reduction in H_{32} and a corresponding 2.5% increase in profile loss due to wake mixing. Therefore, change in the circumferential shape of the boundary layer profile can only explain 2.5% of the 5.1% rise in the profile loss. The remainder is thus attributed to the longer blade and therefore spanwise length of the boundary layer in the case of the 34° design due to the effect of the increased compound lean and sweep.

It is clear that the effect of the transverse pressure gradient is to increase profile loss at design incidence. From these results it is recommended that designers should therefore use the lowest level of lean and sweep that can achieve the blade's required operating range.

5 Uncertainty in Real Design

A compressor designer traditionally has one aerodynamic aim - to maximise design performance while maintaining the required incidence range for operability. In reality there is a second and more important behaviour driving design: “risk”. In the search for design performance a designer may wish to increase pitch-chord ratio or reduce the amount of compound lean. However, such a choice risks catastrophic aerodynamic failure. In practice the designer is likely to react to this risk by “playing safe”. In other words, in practice a fear of “risk”, a lack of understanding of uncertainty, is what inhibits innovative designs.

In this section the compressor design space is studied using both experiments and numerical simulations to investigate the level of uncertainty. Two aerodynamic parameters are varied, the overall blade loading and the strength of the transverse pressure gradient. This is achieved by varying two design parameters: the pitch-chord ratio and the 3D stacking through lean and sweep. The design space is interpreted using the mechanisms governing the aerodynamic 3D failure modes and loss generation described earlier in the paper.

The Design Space

The effects of varying pitch-chord ratio on design performance and incidence range will be introduced first. Figure 17 shows 3D CFD predictions of the design point loss variation with pitch-chord ratio and compound lean and sweep. The effect of raising pitch-chord ratio can be seen to reduce design loss. For an increase in pitch-chord ratio of 16% a reduction in loss of 7.5% is observed. This is due to two effects. First, the increase in overall blade loading increases the entropy created in the boundary layer of the blade. Second, as pitch-chord ratio is increased endwall loss rises. A line of optimum designs exists at 6° of compound lean to minimise the loss. As lean is increased from 6° the design performance drops. This is causes by the increased transverse pressure gradient increasing wake mixing loss downstream of the blade, as discussed earlier in the paper.

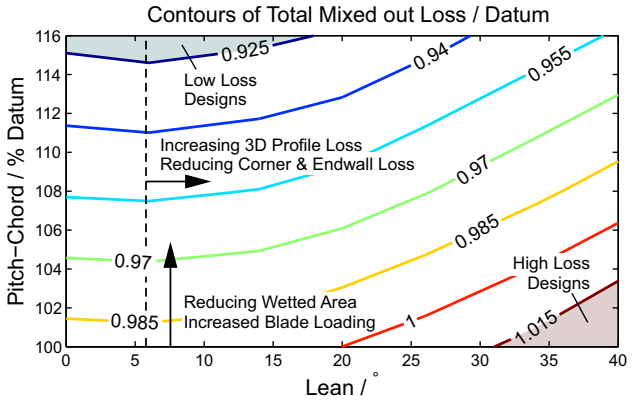

Fig. 17. DESIGN SPACE: DESIGN INCIDENCE LOSS (CFD)

The incidence range across the whole design space, predicted by CFD, is shown in Figure 18. Two clear trends can be observed: first, at a fixed pitch-chord ratio there is a clear optimal level of lean which achieves the maximum operating range (20° lean). Second, at a fixed lean, increasing the pitch-chord ratio always reduced the operating range. The optimal lean which achieves maximum incidence range represents a divide betweeen two regions: The first region is where the blade fails by an open corner separation, the second is where the blade fails by a trailing edge separation. The optimal design for incidence range occurs where the correct selection of the strength of the transverse pressure gradient balances these two mechanisms.

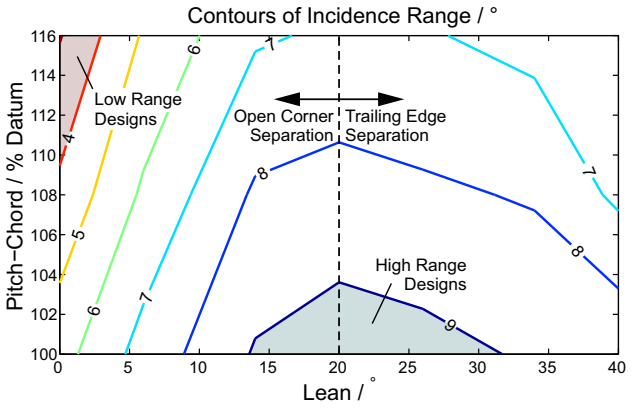

Fig. 18. DESIGN SPACE: POSITIVE INCIDENCE RANGE (CFD)

Figures 17 and 18 show that if a designer wanted to maximise incidence range then they should design with 20° of lean and low values of pitch-chord ratio. While if they wanted to maximise design performance they should design with 6° of lean and high pitch-chord ratio. Both of these views of the design space, however, do not consider the ”risk” of a given design.

Uncertainty in the ability of the CFD to predict the outcome of the experimental tests was observed to vary across the design space; two distinct regions were found with very different uncertainty. The two regions were found to correlate with the type of failure mechanism. In the first region, where open corner separations control the incidence range, the uncertainty was found to be high with even small changes in inlet condition significantly changing the flow structure in the experimental test. In the second region, where trailing edge separations control the incidence range, the uncertainty was found to be low with the trends in the CFD and experiment agreeing closely. In order to quantify the uncertainties in these two regions of the design space a study was conducted by imposing small variations of inlet condition onto the CFD solutions, the results are presented at the end of this section.

Low Risk Region

Over the entire "low risk" region ($> 20^\circ$ lean) the CFD was found to accurately predict the trends of design loss and incidence range. Both experiments and CFD were found to fail by a progressive trailing edge separation.

The experiment and CFD results for the 34° lean, 108% pitch-chord ratio design are shown in Figure 19. The loss coefficients from stator inlet and exit traverses are shown at exit for three incidences. The CFD was found to predict the development of trailing edge separation as incidence was raised. The spanwise location of the initial separation point was also found to be accurately predicted.

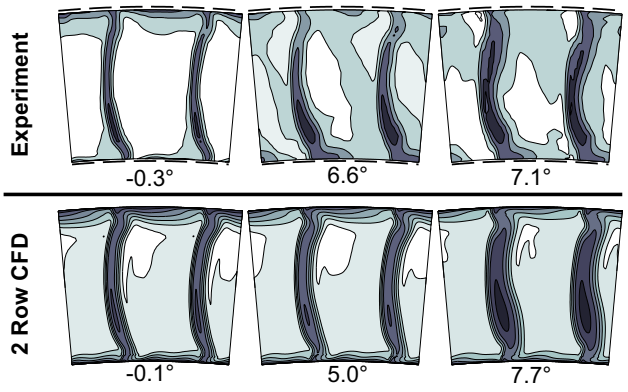

Fig. 19. STATOR EXIT LOSS TRAVERSES IN THE "LOW RISK" REGION OF THE DESIGN SPACE (CFD+EXP)

High Risk Region

Over the entire "high risk" region ($< 20^\circ$ lean) significant discrepancies were observed between the CFD and experiment. In terms of the failure mechanism discussed earlier in the paper the biggest discrepancy was found to be the wall on which the open corner separation occurred.

To demonstrate this effect a single case will be presented. This case is characteristic of a designer attempting use lean and sweep to minimise design loss. In such a case the CFD indicates that the it would be sensible to reduce lean to 6° and increase pitch-chord ratio to 108% of the datum. The CFD predicts that these two choices combined reduce the total loss coefficient by 4.7% of the datum value.

The experiment and CFD for the 6° lean, 108% pitch-chord ratio case is shown in Figure 20. The stator exit traverse at three incidences is shown in the first two rows of the figure. The first two incidences were selected to be the same for both CFD and experiment. The third was selected to be above the critical incidence, where the corner separation had just opened. The CFD is observed to accurately predict the experiment at the lower two incidences. However, at high incidences the CFD predicts the open corner separation occurring on the hub wall, instead of the casing, and at the wrong incidence by 1.4°.

In the experiment the mechanism by which the corner separation opens on the casing wall is identical to that on

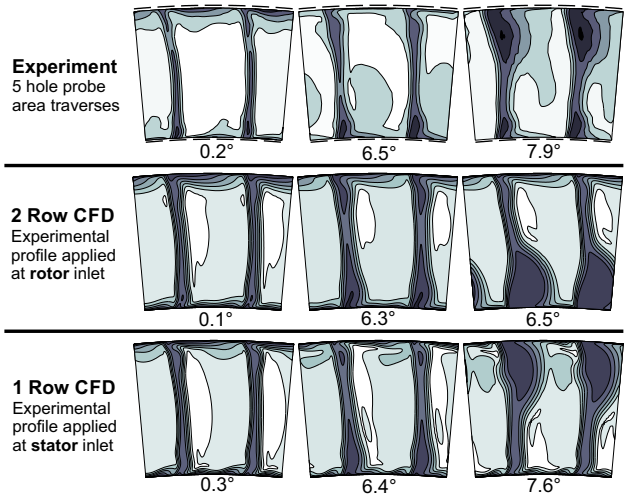

Fig. 20. STATOR EXIT LOSS TRAVERSES IN THE "HIGH RISK" REGION OF THE DESIGN SPACE (CFD+EXP)

the hub wall described by the CFD earlier in the paper. To confirm this result surface flow visualisation was undertaken, two photographs are shown in Figure 21. One is just below and the other is just above the critical incidence. The high streamline curvature below the critical incidence and the existence of the separation surface of the open corner separation above the critical incidence are demonstrated.

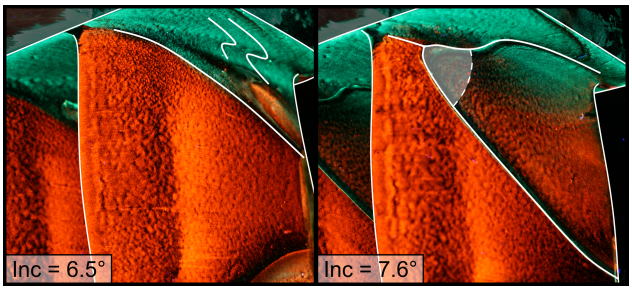

Fig. 21. SURFACE FLOW VISUALIZATION SHOWING THE CREATION OF THE SEPARATION SURFACE (EXP)

The cause of the significant discrepancy between the CFD and experiment was found to be a small difference in the stator inlet flow. This is shown in Figure 22. The difference is only 2° and occurs at 90% span. The CFD was set up with the experimentally measured profile at rotor inlet. The 2° difference at stator inlet is caused by inaccuracies in the RANS modelling of the rotor tip leakage flow. It should also be noted that the meshes used in this study are of a higher fidelity than would used in design. This finding is significant as it shows that even one blade row into a solution the small errors in modelling can cause gross inaccuracies in the prediction of open corner separations.

To confirm the theory that the 2° error in stator incidence close to the casing was the cause of CFD inaccuracy in the stator row, a single row CFD solution was run of the stator alone. The stator inlet condition at each incidence was set

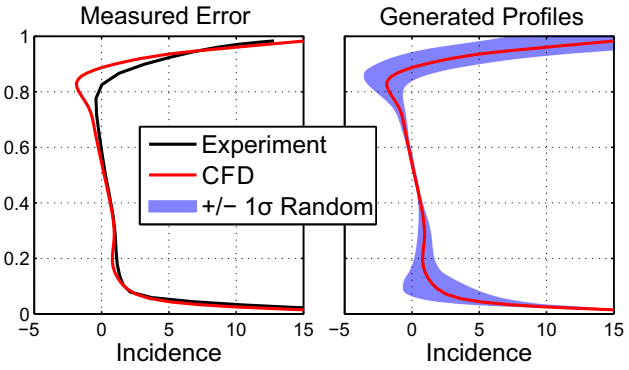

Fig. 22. VARIATION OF STATOR INLET INCIDENCE. LEFT: TEST FACILITY. RIGHT: CFD UNCERTAINTY STUDY (CFD+EXP)

using the experimental rotor exit traverses. The solution is plotted as the third row in Figure 20. It can be seen that the CFD and experiment now agree: The open corner separation occurs on the casing wall and the midspan incidence at which the closed corner separation opens is accurately predicted.

The conclusion from these results is clear. In the "high risk" region, where failure is due to opening of a corner separation, the behaviour of the flow in a given row exhibits extreme sensitivity to the stator inlet conditions. In the case of a real multi-stage machine a greater uncertainty in the inlet profiles exists than that presented here. This increased uncertainty is due to the difficulty in measuring the profiles in a high speed machine, imperfect knowledge of the geometry and the cumulative errors that are built up in a multi-stage CFD calculation used for design.

Design Space Uncertainty

The design space is split into two regions with different levels of uncertainty. Designs with low magnitudes of transverse pressure gradient which fail by open corner separation and designs with high levels of transverse pressure gradient which fail by trailing edge separation. It is the aim of this section to quantify the uncertainty that spans the design space.

The right hand part of Figure 22 shows the mean and standard deviation of flow angle at stator inlet of the set of profiles used in the uncertainty study. The profiles were generated by stretching and scaling the nominal profile by random 5^{th} order polynomials. The method ensured that the uncertainty was raised close to the endwalls to simulate the rise in uncertainty experienced in the experimental testing. The mean of the random profile set is equal to the nominal profile.

Figure 23 shows the uncertainty in the 'loss loops' for two cases, 6° and 34° lean. The two cases chosen are those which were shown previously in Figure 19 and 20. It can be seen that in the 6° lean case there is a significantly greater uncertainty. This is caused by a fundamental sensitivity of the flow topology to small changes inlet condition. The standard deviation (σ) in incidence range of the blade is 1.7° for the 6° design while it is 0.6° for the 34° lean design. It is also important to note that in the case of the 6° design the uncertainty is highly non-linear; the mean incidence range of the random set is 1° lower that the nominal design case.

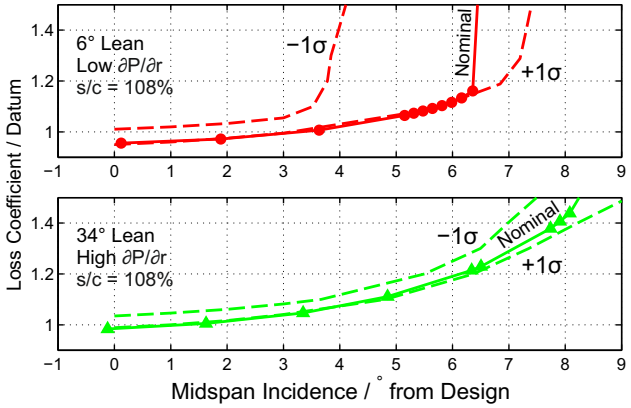

Fig. 23. UNCERTAINTY IN THE LOSS LOOPS DUE TO VARIATION IN INLET PROFILE (CFD)

The inlet profiles of Figure 22 were used to explore the rest of the design space and the results are presented in Figure 24. The first point of note is that the contours are vertical. This indicates that uncertainty, to a first order is not affected by choice of pitch-chord ratio. The divide between the high risk and low risk regions can be seen clearly at a lean of approximately 20°. All designs with a lean greater than 20° experience an uncertainty of a standard deviation that is less than 10% of their nominal incidence range, in this region of the design space the failure is the result of a trailing edge separation. The designs with a low transverse pressure gradient and low lean experience an uncertainty of up to 40% of their nominal incidence range, in this region of the design space the failure is by opening of the corner separation.

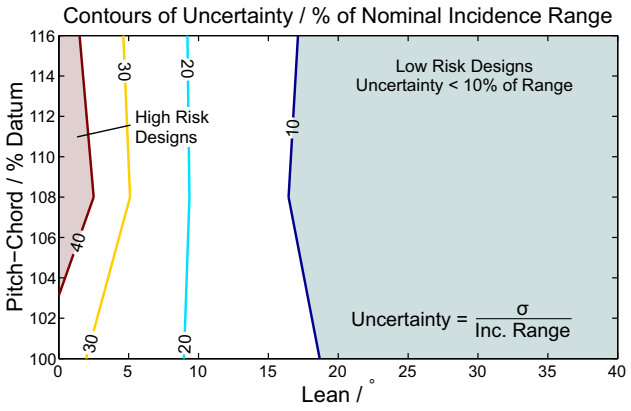

Fig. 24. DESIGN SPACE: UNCERTAINTY OF POSITIVE INCIDENCE RANGE (CFD)

We can now return to the question of the designer's objectives, but this time considering the "risk". If a designer wanted to maximise incidence range then they should design

at 20° of lean and low values of pitch-chord ratio. However, to minimise "risk" they should choose to move further into the "low risk" region by slightly raising lean to perhaps 25° lean. If a designer did not require much incidence range and wanted to maximise design performance they may think that they could reduce lean to 6° and raise pitch-chord ratio. However, this would significantly raise the "risk", moving the design far into the "high risk" region. In order to achieve success in this region they would need to undertake an extensive experimental program to validate their designs.

Conclusions

This paper has shown that the strength of the transverse pressure gradient, as determined by the magnitude of the 3D stacking, is critical in controlling both the failure mechanism and loss of a given design.

It has shown that the inception of critical points at high incidence triggers the opening of a closed corner separation. A saddle point and focus pair form at a point on the blade surface where the curvature of the limiting streamlines is infinitely sharp. These two points then move apart, forming the open corner separation bubble. A new parameter has been developed, the "corner shape factor", based upon the curvature of the limiting streamlines in this region. It can be extracted from either experimental flow visualisation or CFD. It can be used to quantify how close a given design is to forming an open separation at a given inlet condition.

It has also been shown that the separation of the boundary layer from the trailing edge, a phenomenon often treated as 2D, is highly dependant on the strength of pressure gradient transverse to the flow. A strong pressure gradient causes differential overturning of the suction surface boundary layer. This mechanism increases the boundary layer shape factor locally and therefore induces premature trailing edge separation.

Finally, it has been shown that increasing the strength of the transverse pressure gradient (increased lean) of a design increases the total loss at design incidence. The higher loss is attributed to an increase in the profile loss. This is caused by strong transverse pressure gradients reducing H_{32} of the boundary layer, resulting in an increased mixing loss downstream of the blade.

It has been shown that uncertainty in the performance of a compressor design is due to uncertainty in the knowledge of the flow in the endwall region of the blade. In this work an error of 2° in whirl angle at inlet to the stator was found between the CFD prediction and the experiment. This discrepancy in inlet condition close to the casing caused uncertainty to vary across the design space depending on the lean of the different blade designs.

In the "high risk" region of the design space, where lean angles are less than 20°, the failure is due to open corner separation. These designs exhibited extreme sensitivity to the stator inlet conditions with the corner separation sometimes predicted on the casing side, sometimes on the hub. It is clear that in order to succeed in this region a designer must be well informed by experiment.

In the "low risk" region of the design space, where lean angles are greater than 20°, the failure is due to trailing edge separation. These designs exhibited a lower sensitivity to inlet condition. This region offers a safer mode of operation for designers to choose, however, this is at the expense of increased design loss.

An important finding of this paper is that improved management of uncertainty can only be achieved through experimental testing. With modern manufacturing techniques it is possible to test a new design in 1-2 days. In order to capitalise on this, current trends of moving facilities away from designers need to be reversed.

Acknowledgements

The authors would like to thank Rolls-Royce plc for their contributions and permission to publish this work, Chris Hall, Ian Bousfield, Simon Gallimore and Nicholas Cumpsty for their invaluable advice, the EPSRC for their support, TURBOSTREAM for the use of their solver and Graham Pullan for his comments on 3D thinking.

References

[1] Lei, V.-M., Spakovszky, Z. S., and Greitzer, E. M., 2008. "A criterion for axial compressor hub-corner stall". *ASME J. Turbomach.,* **130**(3), May, pp. 031006–031006.

[2] Gallimore, S. J., Bolger, J. J., Cumpsty, N. A., Taylor, M. J., Wright, P. I., and Place, J. M. M., 2002. "The use of sweep and dihedral in multistage axial flow compressor blading part 1: University research and methods development". *ASME J. Turbomach.,* **124**(4), Nov., pp. 521–532.

[3] Brandvik, T., and Pullan, G., 2010. "An accelerated 3D Navier Stokes solver for flows in turbomachines". *ASME J. Turbomach.,* **133**(2), Oct., pp. 021025–021025.

[4] Spalart, P., and Allmaras, S., 1992. "A one equation turbulence model for aerodynamic flows.". *AIAA Journal,* **94-439**, pp. –.

[5] Délery, J., 2013. *Three-dimensional Separated Flow Topology*. ISTE Ltd and John Wiley & Sons Inc.

[6] Poincaré, H., 1891. "Les points singuliers des équations differéntielles". *Comptes-Rendus de l'Académie des Science*.

[7] Gbadebo, S. A., Cumpsty, N. A., and Hynes, T. P., 2005. "Three-dimensional separations in axial compressors". *ASME J. Turbomach.,* **127**(2), May, pp. 331–339.

[8] Rotta, J., 1970. *Eine Beziehung Zwischen den Örtlichen Reibungsbeiwerten Turbulenter Grenzschichten bei Kompressibler und Inkompressibler Strömung*. ZFW.

[9] Wieghardt, K., 1945. *Turbulente Grenzschichten*. Göttinger Monographie.

[10] Schlichting, H., and Gersten, K., 1999. *Boundary Layer Theory*. Springer.